MedChemComm

RESEARCH ARTICLE

View Article Online
View Journal | View Issue

Cite this: *Med. Chem. Commun.*, 2018, **9**, 1164

Curcumin-based pyrazoline analogues as selective inhibitors of human monoamine oxidase A†

Chandrani Nath,[a] Vishnu Nayak Badavath,[a] Abhishek Thakur,[c] Gulberk Ucar,*[b] Orlando Acevedo,*[c] Mohd Usman Mohd Siddique[a] and Venkatesan Jayaprakash*[a]

Received 12th April 2018,
Accepted 6th June 2018

DOI: 10.1039/c8md00196k

rsc.li/medchemcomm

A series of 2-methoxy-4-(5-phenyl-4,5-dihydro-1*H*-pyrazol-3-yl)phenol (pyrazoline) derivatives (**2**–**6**) have been synthesized and tested for human monoamine oxidase (hMAO) inhibitory activity. The most active derivative (**2**) behaved as a competitive hMAO-A inhibitor, with an inhibition constant value of 0.08 μM and a strong hMAO-A selectivity (K_i(hMAO-B)/K_i(hMAO-A) > 1751). In addition, **2** exhibited little to no cytotoxic effects up to a 25 μM concentration and provided the best blood–brain barrier permeability among the derivatives synthesized. Molecular dynamics simulations revealed that a chlorine substituent at the *para*-position of the phenyl ring in **2** enabled a π–π stacking interaction with Tyr407 and Tyr444 that resulted in the formation of an "aromatic sandwich" structure. Consequently, this tight-binding aromatic cage culminated in a dramatically reduced active site volume that is believed to be the origin of the observed selectivity between the hMAO-A and hMAO-B isozymes. Removal of the chlorine from **2** disrupted the favorable intermolecular interactions and resulted in a selectivity change towards hMAO-B.

Introduction

The use of monoamine oxidase inhibitors (MAOIs) as an effective treatment for depression dates back to the 1950s.[1–4] The subsequent decades marked the discovery of more potent inhibitors that provided enhanced selectivity between isozymes MAO-A and MAO-B and had reversible binding with MAO.[5] However, safety concerns have markedly decreased their use in recent years, necessitating the search for alternative MAOIs.[5–7] Accordingly, our group has reported novel MAOIs that mimic the structural features of curcumin, a natural polyphenol known for its MAO inhibitory activity.[8,9] An additional class of MAOIs was also reported featuring pyrazoline derivatives synthesized from chalcones resembling curcumin with normal and reversed α,β-unsaturated carbonyl functionalities.[10,11] Both of these compound classes displayed a similar activity profile. In continuation of our earlier efforts, novel analogues are reported in this work that feature variations in the phenyl ring at C5 carbon of pyrazoline (Fig. 1). Five new pyrazoline derivatives encompassing a chlorine substitution at the *para*-position were synthesized and tested for hMAO-inhibitory activity. In addition, the compounds were evaluated for cytotoxicity and permeability characteristics. Computational docking and molecular dynamics (MD) simulations were performed to provide atomistic insight into the potent activity and large selectivity measured for compound **2**.

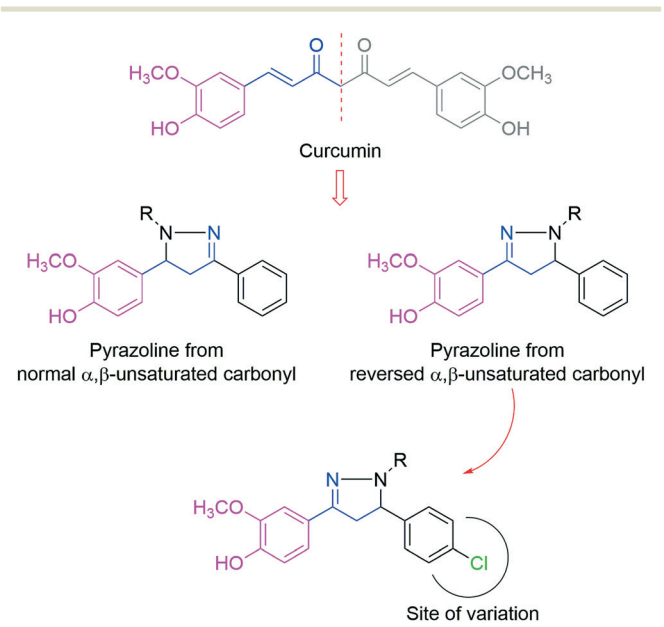

Fig. 1 Design strategy adopted for designing MAO inhibitors.

[a] *Department of Pharmaceutical Sciences & Technology, Birla Institute of Technology, Mesra, Ranchi-835 215, Jharkhand, India. E-mail: drvenkatesanj@gmail.com; Tel: +91 9470137264*
[b] *Department of Biochemistry, Faculty of Pharmacy, Hacettepe University, Sıhhiye 06100, Ankara, Turkey*
[c] *Department of Chemistry, University of Miami, Coral Gables, Florida 33146, USA. E-mail: orlando.acevedo@miami.edu; Tel: +1 305 284 5662*

† Electronic supplementary information (ESI) available. See DOI: 10.1039/c8md00196k

Results and discussion

Synthesis and characterization

Through the reactions outlined in the Scheme 1, five novel pyrazoline derivatives (**2–6**) were synthesized adopting the protocol reported earlier.[10,11] Condensation of **1** with hydrazine hydrate in ethanol provided the intermediate pyrazoline (**2**), which is required for the synthesis of other derivatives (**3–6**). Reaction of **2** with benzoyl chloride, toluene sulfonyl chloride, phenyl chloroformate, and phenyl isothiocyanate provided **3**, **4**, **5** and **6**, respectively. The reaction procedures and characterization data for all compounds are presented in the ESI.†

Compounds **2–6** were characterized by ^{1}H-NMR and ESI-MS spectra. Three protons in the C4 and C5 positions of pyrazoline exhibited three doublet-of-doublets (dd) in ^{1}H-NMR that is characteristic of this class of compounds. Two dd appeared in the region δ2.716–3.872 ppm and δ3.852–3.926 ppm, respectively for two H's at the C4 position of pyrazoline. The third dd for the H at C5 position of pyrazoline appeared in the δ4.739–6.006 ppm region. At δ3.756–3.834 ppm a sharp singlet for Ar–OCH_3 was found and at δ9.590–9.950 ppm a singlet for Ar–OH of the vanillyl head appeared. The tolyl-CH_3 peak of compound **4** gave a singlet at δ2.226 ppm. The peak for the –NH– proton of compound **2** appeared at δ10.04 ppm. ESI-MS spectra of all the final compounds displayed the characteristic molecular ion peak (M^+).

Inhibitory activity, selectivity, and reversibility

The newly synthesized pyrazoline derivatives were screened for their inhibitory activity of hMAO isoforms by using recombinant enzymes. Recombinant enzymes and the other chemicals were purchased from Sigma-Aldrich (Munich, Germany). The Amplex®-Red MAO assay kit was obtained from Molecular Probes, USA. Enzyme activities were determined by utilizing the Amplex Red MAO assay kit (ESI†). The novel compounds and the known inhibitors tested did not interfere with the measurements or interact with resorufin as the fluorescence signal did not change when the compounds were treated with various concentrations of resorufin. The experimental results are given in Table 1. Selectivity indexes (SI) were expressed as the inhibition constant ratio K_i(hMAO-B)/K_i(hMAO-A). Selectivity towards hMAO-A increases as the corresponding SI increases; conversely, the selectivity towards hMAO-B isoform increases as the corresponding SI decreases.

The mode of hMAO inhibition was examined using a Lineweaver–Burk plot (Fig. 2). The slopes of each Lineweaver–Burk plot were plotted *versus* the inhibitor concentration [*I*], which allowed the inhibition constant (K_i) values to be computed from the *x*-axis intercept as $-K_i$. Reversibility of hMAO inhibition with the compounds was determined by a previously described dialysis method (ESI†). All compounds selectively inhibited hMAO-A. While compounds **2–6** inhibited hMAO-A in the 0.080–192.84 μM concentration range, the majority (with the exception of **2**) did not inhibit hMAO-B even at concentrations near 5000 μM. Among the newly synthesized pyrazoline derivatives, **2**, which carries no substitution on 1*N*, was the most potent hMAO-A inhibitor with a K_i value of 0.080 ± 0.009 μM. Compound **2** inhibited hMAO-A more potently than moclobemide, a selective, potent, and reversible hMAO-A inhibitor[12] with a measured K_i value of 0.102 ± 0.009 μM (Table 1). It was surprising

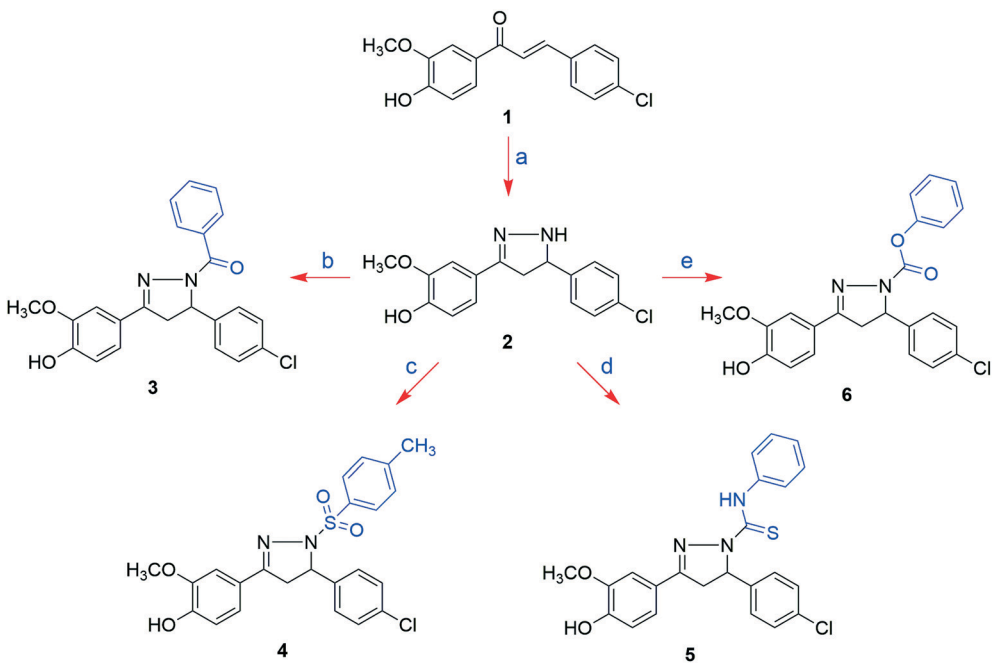

Scheme 1 Reagents and conditions: (a). $NH_2NH_2{\cdot}H_2O$, EtOH, 90 °C, 3–6 h; (b). C_6H_5COCl, pyridine, 100 °C 3–4 h; (c). *p*-CH_3–$C_6H_4SO_2Cl$, THF, 10–15 min, 10–15 °C; (d). C_6H_5–NCS, EtOH, reflux, 2–3 h; (e). Cl–CO–OC_6H_5, K_2CO_3, EtOH, 30 min < 10 °C.

Table 1 Experimental K_i values for hMAO inhibitory activities of 2-methoxy-4-(5-phenyl-4, 5-dihydro-1*H*-pyrazol-3-yl) phenol derivatives

Code	K_i value (μM)[a]		SI	Inhibition type	Reversibility	MAO selectivity
	hMAO-A	hMAO-B				
2	0.080 ± 0.009	140.10 ± 12.00	1751.25	Competitive	Reversible	**A**
3	26.20 ± 0.09	6000.00 ± 97.00	229.01	Competitive	Reversible	A
4	40.00 ± 0.11	6000.00 ± 12.00	150.00	Competitive	Reversible	A
5	19.55 ± 12.20	4770.16 ± 99.00	244.00	Competitive	Reversible	A
6	192.84 ± 17.16	5771.00 ± 95.00	29.93	Competitive	Reversible	A
Sel	3.60 ± 0.19	0.255 ± 0.010	0.07	Suicide inhibitor	Irreversible	B
Laz	7900.00 ± 66.11	0.006 ± 0.001	7.59×10^{-7}	Competitive	Reversible	B
Moc	0.102 ± 0.009	4.22 ± 0.11	41.37	Competitive	Reversible	A

[a] Values are expressed as the mean ± SEM (n = 3). SI: Selectivity index is calculated as K_i(hMAO-B)/K_i(hMAO-A). Sel: Selegiline; Laz: lazabemide; Moc: moclobemide.

to find that compound **2** displayed such strong hMAO-A inhibitory activity as an analogue lacking the chlorine substituent (**4*** in Scheme 2) was reported in earlier work to be a selective inhibitor of hMAO-B.[10,11] Moreover, **2** was found to be better than the **3–6** counterparts possessing bulkier substituents at the 1*N* position.

The selectivity of compound **2** towards hMAO-A also was also found to be better (SI = 1751.25) than that of moclobemide (SI = 41.37). For the kinetic experiments, the reaction velocities of hMAO-A and hMAO-B at different *p*-tyramine concentrations were measured. Lineweaver–Burk graphs were constructed in the absence of inhibitor and in the presence of reference and novel inhibitors (Fig. 2). Since the lines are linear and intersect on the *y*-axis, all compounds in this series are suggested to be competitive inhibitors of hMAO isoforms, which may interact within the catalytic site of the enzymes. The selectivities of compounds **3**, **4**, and **5** for hMAO-A also were found to be better than that of moclobemide (Table 1). The reversibility of hMAO inhibition by compounds **2–6** was investigated by measuring the recovery of hMAO activity after dialysis of enzyme–inhibitor mixtures. Isoforms of hMAO were incubated in the presence of the representative inhibitors at concentrations equal to five-fold that of the K_i values for a period of 15 min and then subsequently dialyzed for 24 h. hMAO-A inhibition by the new compounds were almost completely reversed after 24 h of dialysis suggesting that **2–6** are reversible inhibitors of hMAO (ESI†).

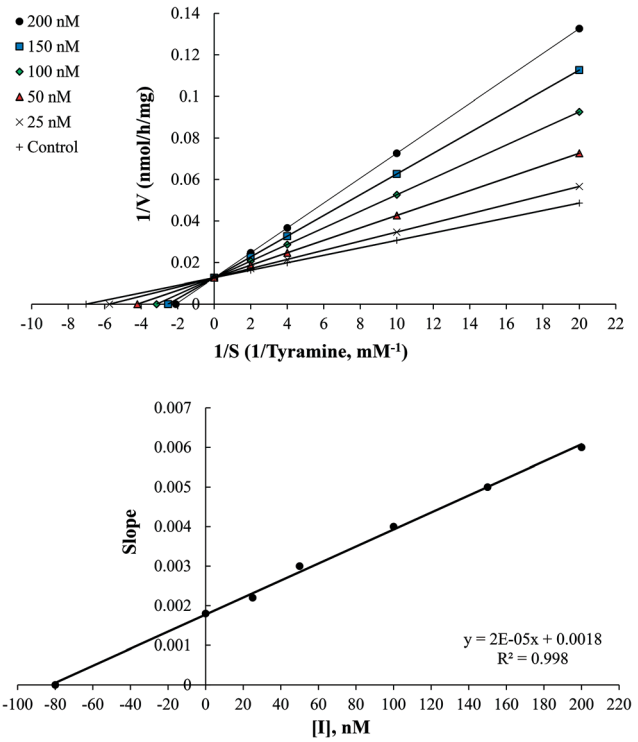

Fig. 2 Lineweaver–Burk plots for the inhibition of hMAO-A by compound **2**. [*S*], substrate concentration [mM]; *V*, reaction velocity [nmol h^{-1} mg^{-1}]; K_i, inhibition constant; R^2, coefficient of determination. Inhibitor concentrations [*I*] are shown in legend. The bottom graph represents the plots of the slopes of the Lineweaver–Burk plots (*y*) *versus* inhibitor concentrations (*x*). K_i was calculated as 80.00 nM.

As cyclization of chalcone with hydrazine generates a chiral center at the C5 position of pyrazoline, the compounds were obtained as mixture of enantiomers. Specific rotation of the racemic compounds were determined and that was followed by chiral separation using an analytical chiral column to access enantiomeric ratio. Compound **2** was found to have both enantiomers in equal proportion, while **3–6** had one enantiomer in 93.5–98.8% excess. The activity of compounds **3–6** may be attributed to a single isomer whose configuration is unknown at present. In contrast, enantiomers of compound **2** were found to be in equal proportion and one of them must be contributing to the potent MAO-A inhibitory activity. Hence, study on chiral separation, the determination of configuration for each enantiomer, and their inhibitory activity against hMAO-A is warranted. In the present work no attempt was made to separate the two isomers; instead, a

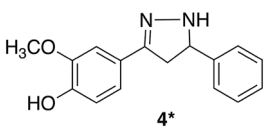

4*

Scheme 2 2-Methoxy-4-(5-phenyl-4,5-dihydro-1*H*-pyrazol-3-yl)-phenol hMAO inhibitor reported in ref. 10.

Table 2 *In vitro* cytotoxicity of newly synthesized 2-methoxy-4-(5-phenyl-4,5-dihydro-1*H*-pyrazol-3-yl) phenol derivatives

	Viability (%)		
Code	1 μM	5 μM	25 μM
2	99.00 ± 1.78	94.55 ± 3.09	90.22 ± 1.57
3	90.02 ± 2.16	86.29 ± 2.01	78.22 ± 1.07
4	91.20 ± 2.88	79.55 ± 1.84*	64.10 ± 1.67**
5	95.04 ± 2.33	88.21 ± 2.04	80.35 ± 1.74
6	93.10 ± 2.11	81.70 ± 1.55	77.00 ± 1.25

Data are expressed as mean ± SEM (n = 3). Cell viability is expressed as a percentage of the control value. $p < 0.05$ is considered as statistically significant (*$p < 0.05$, **$p < 0.01$, ***$p < 0.001$ *vs.* control).

computational approach has been employed to check the effect of chirality on activity and selectivity (see "Computational studies" section).

Cytotoxicity and permeability

The *in vitro* cytotoxicity of compounds **2–6** was tested in HepG2 cells at three different concentrations, *i.e.*, 1, 5, and 25 μM, (Table 2). The HepG2 cell line was purchased from the American Tissue Culture Collection (ATCC®; catalog no. HB-8065; Manassas, VA, Invitrogen). All compounds were found to be non-toxic to hepatic cells at 1 μM concentration and **2** was found to display ~90% viability for hepatic cells even at 25 μM concentration.

Further, the compounds were tested for their ability to cross blood–brain barrier (BBB). A parallel artificial membrane permeation assay of blood–brain barrier (PAMPA-BBB) was performed. The assay was validated through a comparison of reported permeability values of commercially available drugs (Table 3). A plot of experimental data *versus* literature values gave a good linear correlation (R^2 = 0.9935). Reference compounds were classified according to the limits previously reported.[13] The data indicated that the selected derivatives **2**, **4**, and **5** can cross the BBB (Table 3). Compounds **2** and **4** showed the highest permeability suggesting that they may cross the BBB easily and reach biological targets located in the Central Nervous System (CNS).

Computational studies

Docking and molecular dynamics (MD) simulations were carried out to understand the effect of chirality and other structural features that determine the potency and selectivity of compound **2**. This approach has been successfully applied in earlier works.[14–20] Complexes of hMAO-A bound with the *R*- and *S*-conformers of compounds **2** and **4*** were studied, as **2** was the most potent compound and possessed a high selectivity towards hMAO-A, whereas **4*** (from ref. 10) was selective towards hMAO-B despite sharing the same scaffold minus the chlorine substituent (Scheme 2). The X-ray crystal structure of hMAO-A co-crystallized with harmine (PDB: 2Z5X) has been used to generate the initial coordinates needed to perform the simulation studies. Protein–ligand complexes for all four ligands (2*R*, 2*S*, 4**R*, 4**S*) were prepared from the output of molecular docking calculations and subjected to molecular dynamics simulations.

The root-mean-square deviation (RMSD) of the backbone protein atoms were calculated for each hMAO-A/ligand complex over the entire 100 ns trajectory from each MD simulation. The RMSD plots showed that the hMAO-A system bound to 2*R* became very stable after 20 ns in contrast to the 2*S* bound system, which presented larger variations over the entire simulation (Fig. 3). The 4**R* and 4**S*, showed much more dramatic geometry variations over the course of the computed trajectory, indicating that the Cl atom may provide significant stabilization within the binding pocket. Root-mean-square fluctuation (RMSF) calculations can help elucidate the dynamical response to ligand binding (Fig. 4). Visual inspection of the RMSF plot finds that 2*R* has very low fluctuations,

Table 3 Permeability data obtained from the PAMPA-BBB assay for the selected newly synthesized 2-methoxy-4-(5-phenyl-4,5-dihydro-1*H*-pyrazol-3-yl) phenol derivatives and commercial drugs used in the validation of the assay

Compounds[a]	Bibliography[b] Pe ($\times 10^{-6}$ cm s^{-1})[c]	Experimental Pe ($\times 10^{-6}$ cm s^{-1})[c]	Prediction
Testosterone	17.0	16.22 ± 1.80	CNS+
Verapamil	16.0	15.02 ±1.17	CNS+
β-Estradiol	12.0	11.85 ±0.96	CNS+
Progesterone	9.3	9.50 ± 0.61	CNS+
Corticosterone	5.1	4.98 ± 0.19	CNS+
Piroxicam	2.5	2.64 ± 0.14	CNS±
Hydrocortisone	1.8	1.80± 0.13	CNS−
Lomefloxacin	1.1	1.24 ± 0.02	CNS−
Dopamine	0.2	0.22 ± 0.01	CNS−
2		13.86 ± 0.99	CNS+
4		12.01 ± 1.00	CNS+
5		9.55 ± 0.41	CNS+

[a] Compounds were dissolved in DMSO at 2 mg m^{-1} land diluted with PBS/EtOH (70 : 30). The final concentration of compounds was 50 μg mL^{-1}. [b] Taken from ref. 14 (Di *et al.*)[13] [c] Values are expressed as the mean ± SEM of three independent experiments. CNS+ (high BBB permeation predicted): Pe (10^{-6} cm s^{-1}) >4.00. CNS− (low BBB permeation predicted): Pe (10^{-6} cm s^{-1}) <2.00. CNS± (BBB permeation uncertain): Pe (10^{-6} cm s^{-1}) from 4.00 to 2.00.

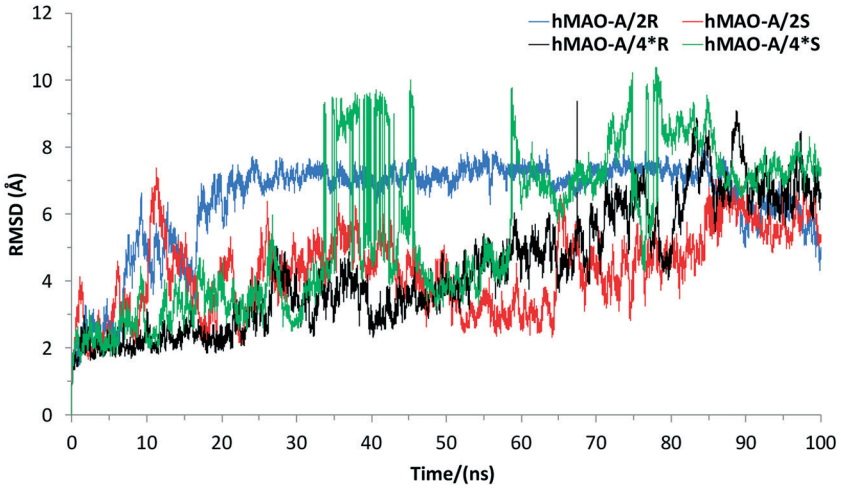

Fig. 3 Root-mean-square deviation (RMSD) of the protein backbone atoms (N, C_α and C) for the respective simulations relative to the first frame.

which is consistent with enhanced stabilization induced by favorable binding of the ligand. The other ligands show more intense movement upon binding compared to 2*R*. The particularly large fluctuations when hMAO-A is bound to the 2*S*-conformer suggests a poor stability associated with the chirality of the ligand.

The MM/PBSA method (ESI†) was utilized to compute the free energy of binding (ΔG_{bind}) for the four ligands bound to hMAO-A (Table 4). 2*R* was found to interact strongly with a ΔG_{bind} of −27.1 kcal mol^{-1}, which is 2.3 kcal mol^{-1} lower in energy in comparison with 2*S*. Both 4**R* and 4**S* had significantly reduced binding affinities relative to 2*R*.

To probe the origin of the hMAO-A preference for the 2*R*, hydrogen bonding population occupancy between the bound ligands and nearby active site residues was monitored over the course of the entire trajectory. It was observed that acceptor oxygen (bb carbonyl oxygen) from Ile180 formed a hydrogen bond population of 72.7% with the hydrogen donor from the pyrazoline ring nitrogen (1*N*) of 2*R*. An average hydrogen bond angle of 160° and a rather lengthy distance of 2.90 Å were computed. A hydrogen bond population of 70.3% was also computed between the acceptor oxygen (bb carbonyl oxygen) from Thr336 and the hydroxy group of 2*R* and with a typical bond length of 2.85 Å and a bond angle of 149° (Fig. 5). The hydroxyl group from 2*S* had reduced hydrogen bonding with the Thr336 as the percent occupancy fell to 43.2% and an average bond length and angle of 3.10 Å and 139°, respectively, were further from ideal values. A hydrogen bond with Ile180 was not observed; however, an interaction with Ile207 yielded a percent occupancy of 84.4% with an average bond length and angle of 3.00 Å and 152°, respectively, for 2*S*.

Unique to the 2*R* binding conformation was a favorable π–π stacking where the chlorine containing phenyl ring was bound in-between the Tyr407 and Tyr444 aromatic cage of hMAO-A (Fig. 5 and 6). This "aromatic sandwich" orientation has been postulated to provide an environment necessary to polarize the substrate amine lone pair to enhance nucleophilicity in the reaction mechanism.[21] In addition, the mutation of Tyr407 → Phe407 and Tyr444 → Phe444 in hMAO-A has been shown to significantly reduce enzymatic activity, whereas a mutation to Ser407 or Ser444 completely killed the activity.[22–24] While the 2*S* and 4**S* ligands did not possess the ideal aromatic "sandwich" orientation found in the 2*R* system, they did have a favorable π–π interaction with Tyr444 (Fig. 5 and 6).

Interestingly, when comparing the computed volume of the harmine binding site region from the hMOA-A crystal structure (PDB ID: 2Z5X) to that of the simulated enzyme

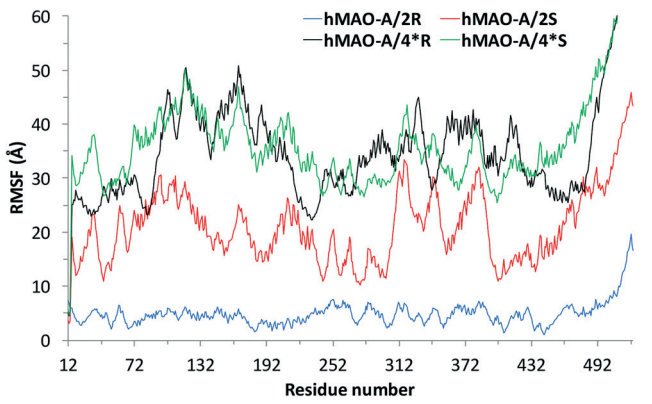

Fig. 4 The root-mean-square fluctuation (RMSF) plot by residue for the hMAO-A complexes using backbone atoms (C, C_α, and N) relative to the lowest energy structure.

Table 4 Computed binding free energies, ΔG_{bind}, (kcal mol^{-1}) using MM/PBSA for the *R* and *S* conformers bound to hMAO-A

Protein–ligand complex	Binding free energy (ΔG_{bind}) kcal mol^{-1}
hMAO-A/2*R*	−27.1
hMAO-A/2*S*	−24.8
hMAO-A/4**R*	−13.1
hMAO-A/4**S*	−18.1

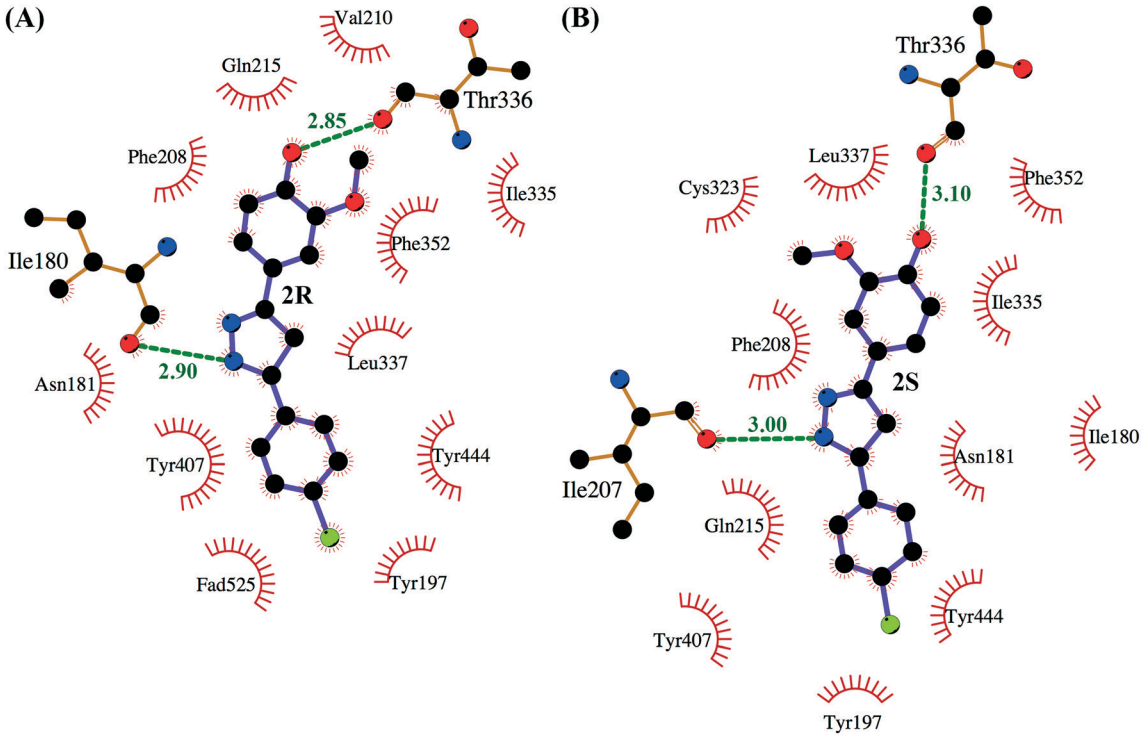

Fig. 5 Active site orientation for (A) hMAO-A/2*R* complex (B) hMOA-A/2*S* complex from molecular dynamics simulations.

bound with 2*R* and 2*S*, it was predicted that 2*R* had a considerably smaller binding pocket (Table 5). The volume was estimated using the software Autoligand on the lowest energy frame of each 100 ns MD simulation. This correlates with the compact "aromatic sandwich" orientation found exclusively for 2*R*.

Computational methodology

Docking. Docking studies were performed using the AutoDock4.2 program,[25] which combines the Lamarckian Genetic Algorithm with an empirical force field to yield fast predictions of binding modes and energies. A grid was centered over the harmine binding region with a box size set at $x = y = z = 30$ grid points. Protein preparation was carried out by removing all crystallographic water molecules, adding polar hydrogens, computing Kollman charges, and assigning atomic radii and AutoDock4 atom types. Docking parameters were created using default values except the exhaustiveness of the global search, which was set to 100. A more detailed description of the computational methodology, including validation of ligand binding poses and the exploration of additional binding sites, is provided in the ESI.†

Molecular dynamics. MD simulations were carried out using the GPU version of Amber 14.[26] Any hydrogen atoms missing in the published crystal structure (PDB: 2Z5X) were reinserted and the protein–ligand complex was explicitly solvated in an orthorhombic TIP3P water box extending 10 Å away from the edges of the protein. Chloride anions were added to neutralize the overall charge of the system. The ff14SB force field[27] was used for the protein and the generalized AMBER force field (GAFF) was used to make topology files for flavin adenine dinucleotide (FAD) and all ligands. Each system was conjugate gradient (CG) minimized for 200 steps for water and ions only, followed by 10 000 steps for the entire system. To calculate the long-range electrostatic potential, the particle-mesh Ewald method was applied and a 12 Å cut-off was employed. The SHAKE algorithm was applied to

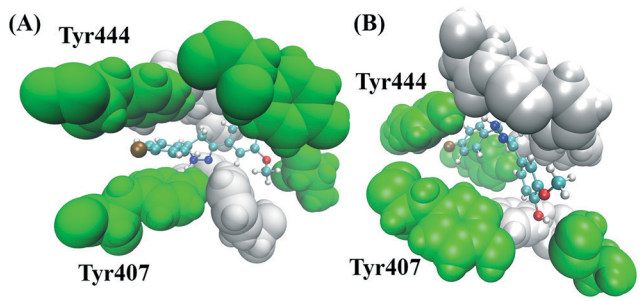

Fig. 6 Active site orientation of hMAO-A bound to (A) 2*R* and (B) 2*S* from molecular dynamics simulations highlighting the role of Tyr444 and Tyr407 in π–π stacking.

Table 5 Volumes calculated for the hMAO-A binding pocket region

Protein–ligand complex	Volume (pm^3)
Crystal structure[a]	4640
hMOA-A/2*R*	3890
hMOA-A/2*S*	6040

[a] PDB ID: 2Z5X.

constrain all bond lengths that included hydrogen atoms to their equilibrium distance. Following minimization, the system was gradually heated from 0 to 300 K with a constant NVT ensemble for 50 ps of MD using the weak-coupling algorithm with a temperature coupling value of 2.8 ps. Thereafter, the system was subjected to a constant NPT ensemble at 300 K and 1 atm for 500 ps with temperature and pressure coupling values of 2.0 ps. The system was then equilibrated using an NVT ensemble for an additional 500 ps. Following equilibration, a production run was collected for 100 ns using the NVT ensemble. Analysis for each system was performed using the cpptraj and ptraj programs within AmberTools.

Conclusions

The current study revealed that 3,5-diphenyl substituted pyrozolines may selectively inhibit hMAO-A when possessing the appropriate substitutions on the phenyl rings. Compound **2** was found to be both potent and highly selective towards hMAO-A with no cytotoxic effects at 1 μM and >90% viability exhibited at 25 μM concentration. In addition, **2** displayed the best BBB permeability among the derivatives synthesized. Molecular dynamics simulations revealed that a chlorine substituent at the *para*-position of the phenyl ring at the 5th position of pyrazoline, improved the π–π stacking interaction with Tyr407 and Tyr444 resulting in an "aromatic sandwich" structure. The *R*-configuration best accommodated the molecule in the active site so as to establish two hydrogen bonding interactions with Thr336 and Ile180. These favorable nonbonded interactions yielded a tight binding between hMAO-A and the *R*-configuration of **2** that gave a significant reduction in the binding pocket volume as compared to the *S*-configuration. 3,5-Diphenyl pyrazolines due to their smaller size as compared to the hMAO-A pocket volume has long been suggested to interact poorly with hMAO-A and hence shift their selectivity towards hMAO-B. However, when appropriately substituted, *i.e.*, *para*-chloro substitution on phenyl ring at C5 and *para*-hydroxy substitution on phenyl ring at C3, these scaffolds can shift back their selectivity toward hMAO-A.

Abbreviations

MAO	Monoamine oxidase
hMAO	Human MAO
SAR	Structure–activity relationship
FAD	Flavin adenine dinucleotide
MAOI	Monoamine oxidase inhibitor

Conflicts of interest

The authors declare no competing interest.

Acknowledgements

Authors acknowledge Central Instrumentation Facility (CIF) and of Birla Institute of Technology and Dr. Reddy's Institute of Life Science, Hyderabad for spectral characterization. C.N. acknowledges the Junior Research Fellowship from the University Grants Commission, New Delhi, India. Gratitude is expressed by A.T. and O.A. to the Center for Computational Science at the University of Miami for support of this research.

References

1 C. R. Conway, M. A. Gebara, M. C. Walker, C. N. Lessov-Schlaggar, A. M. Janski, J. T. Chibnall, P. Cristancho, Y. I. Sheline, B. M. Gott and D. M. Svrakic, *J. Clin. Psychiatry*, 2015, **76**, 1569–1570.
2 S. J. Thomas, M. Shin, M. G. McInnis and J. R. Bostwick, *Pharmacotherapy*, 2015, **35**, 433–449.
3 N. S. Kline and T. B. Cooper, in *Psychotropic Agents: Part I: Antipsychotics and Antidepressants*, ed. F. Hoffmeister and G. Stille, Springer Berlin Heidelberg, Berlin, Heidelberg, 1980, pp. 369–397, DOI: 10.1007/978-3-642-67538-6_17.
4 F. López-Muñoz and C. Álamo, in *Melatonin, Neuroprotective Agents and Antidepressant Therapy*, ed. F. López-Muñoz, V. Srinivasan, D. de Berardis, C. Álamo and T. A. Kato, Springer India, New Delhi, 2016, pp. 365–383, DOI: 10.1007/978-81-322-2803-5_26.
5 K. I. Shulman, N. Herrmann and S. E. Walker, *CNS Drugs*, 2013, **27**, 789–797.
6 S. Carradori and J. P. Petzer, *Expert Opin. Ther. Pat.*, 2015, **25**, 91–110.
7 J. M. Zajecka and A. M. Zajecka, *Psychiatr. Ann.*, 2014, **44**, 513–523.
8 V. N. Badavath, İ. Baysal, G. Ucar, B. N. Sinha, S. K. Mondal and V. Jayaprakash, *J. Pharm. Chem.*, 2015, **2**, 12–17.
9 V. N. Badavath, İ. Baysal, G. Uçar, S. K. Mondal, B. N. Sinha and V. Jayaprakash, *Arch. Pharm.*, 2016, **349**, 9–19.
10 V. N. Badavath, I. p. Baysal, G. Ucar, B. N. Sinha and V. Jayaprakash, *ACS Med. Chem. Lett.*, 2015, **7**, 56–61.
11 V. N. Badavath, G. Ucar, B. N. Sinha, S. K. Mondal and V. Jayaprakash, *ChemistrySelect*, 2016, **1**, 5879–5884.
12 U. Bonnet, *CNS Drug Rev.*, 2003, **9**, 97–140.
13 L. Di, E. H. Kerns, K. Fan, O. J. McConnell and G. T. Carter, *Eur. J. Med. Chem.*, 2003, **38**, 223–232.
14 F. Chimenti, A. Bolasco, F. Manna, D. Secci, P. Chimenti, O. Befani, P. Turini, V. Giovannini, B. Mondovì and R. Cirilli, *J. Med. Chem.*, 2004, **47**, 2071–2074.
15 Z. Özdemir, H. B. Kandilci, B. Gümüşel, Ü. Çalış and A. A. Bilgin, *Eur. J. Med. Chem.*, 2007, **42**, 373–379.
16 F. Chimenti, R. Fioravanti, A. Bolasco, F. Manna, P. Chimenti, D. Secci, F. Rossi, P. Turini, F. Ortuso and S. Alcaro, *Eur. J. Med. Chem.*, 2008, **43**, 2262–2267.
17 A. Sahoo, S. Yabanoglu, B. N. Sinha, G. Ucar, A. Basu and V. Jayaprakash, *Bioorg. Med. Chem. Lett.*, 2010, **20**, 132–136.
18 M. Karuppasamy, M. Mahapatra, S. Yabanoglu, G. Ucar, B. N. Sinha, A. Basu, N. Mishra, A. Sharon, U. Kulandaivelu

and V. Jayaprakash, *Bioorg. Med. Chem.*, 2010, **18**, 1875–1881.
19 M. Jagrat, J. Behera, S. Yabanoglu, A. Ercan, G. Ucar, B. N. Sinha, V. Sankaran, A. Basu and V. Jayaprakash, *Bioorg. Med. Chem. Lett.*, 2011, **21**, 4296–4300.
20 B. V. Nayak, S. Ciftci-Yabanoglu, S. S. Jadav, M. Jagrat, B. N. Sinha, G. Ucar and V. Jayaprakash, *Eur. J. Med. Chem.*, 2013, **69**, 762–767.
21 M. Li, C. Binda, A. Mattevi and D. E. Edmondson, *Biochemistry*, 2006, **45**, 4775–4784.
22 R. K. Nandigama, J. R. Miller and D. E. Edmondson, *Biochemistry*, 2001, **40**, 14839–14846.
23 C. Binda, A. Mattevi and D. E. Edmondson, *J. Biol. Chem.*, 2002, **277**, 23973–23976.
24 R. M. Geha, K. Chen, J. Wouters, F. Ooms and J. C. Shih, *J. Biol. Chem.*, 2002, **277**, 17209–17216.
25 G. M. Morris, R. Huey, W. Lindstrom, M. F. Sanner, R. K. Belew, D. S. Goodsell and A. J. Olson, *J. Comput. Chem.*, 2009, **16**, 2785–2791.
26 R. Salomon-Ferrer, A. W. Goetz, D. Poole, S. Le Grand and R. C. Walker, *J. Chem. Theory Comput.*, 2013, **9**, 3878–3888.
27 J. A. Maier, C. Martinez, K. Kasavajhala, L. Wickstrom, K. E. Hauser and C. Simmerling, *J. Chem. Theory Comput.*, 2015, **11**, 3696–3713.